

Distortion Is Not Noise: On the Limits of the Kappa Model for Monostatic ISAC

Haofan Dong, *Student Member, IEEE*, and Ozgur B. Akan, *Fellow, IEEE*

Abstract—Monostatic ISAC sensing differs from communication because the transmitter can monitor its distorted transmit waveform. Thus, the aggregate κ distortion model, which treats impairments as unknown noise, is appropriate for communication but pessimistic for monostatic sensing. We derive PA-aware sensing Cramér–Rao bounds (CRBs) and a PN-aware CRB that reveals an irreducible velocity-error floor, and quantify when κ -based bounds overestimate sensing degradation. Simulations validate the analysis and show robustness to practical DPD template errors (less than 1 dB overhead at a typical -25 dB NMSE).

Index Terms—Integrated sensing and communication, hardware impairments, Cramér–Rao bound, power amplifier, phase noise, Fisher information.

I. INTRODUCTION

Integrated sensing and communication (ISAC) has emerged as a key enabler for next-generation wireless systems [1]–[3]. A critical practical challenge is the impact of radio-frequency (RF) hardware impairments—particularly power amplifier (PA) nonlinearity and oscillator phase noise (PN)—on joint performance.

The dominant approach models all impairments via the aggregate κ distortion model [4]–[6]: $z = \sqrt{1-\kappa_t^2}x + \eta_t$ with $\eta_t \sim \mathcal{CN}(0, \kappa_t^2 P_X)$, adopted for ISAC analysis [7] and waveform design [8]. Notably, [7] directly applies the κ model to derive sensing SCNR for ISAC precoding, and [8] uses it as the HWI model for end-to-end ISAC learning—both inheriting the “distortion-as-noise” assumption for the sensing echo. However, the κ model assumes the distortion η_t is *unknown* at the receiver. While valid for communication, this is violated in monostatic sensing, where the co-located transmitter knows its own distorted waveform (Fig. 1).

On the physics-based side, Keskin *et al.* [9] derive the PN-aware sensing CRB via the augmented FIM for monostatic OFDM, and our prior work [10] models individual HWI for THz ISAC. However, [9] does not address PA nonlinearity, does not compare against the κ model, and does not establish the separability of PA and PN effects. No prior work systematically compares the κ model against physics-based HWI models for *both* sensing and communication.

The contributions are: (i) a physics-based sensing CRB under PA nonlinearity (Theorem 1), with SNR-independent degradation <1.1 dB, and a proof that the κ model overestimates by a factor growing linearly with SNR (Theorem 2);

H. Dong, and O. B. Akan are with the Internet of Everything Group, Department of Engineering, University of Cambridge, Cambridge CB3 0FA, U.K. (e-mail: hd489@cam.ac.uk; oba21@cam.ac.uk).

Ozgur B. Akan is also with the Center for neXt-generation Communications (CXC), Department of Electrical and Electronics Engineering, Koç University, 34450 Istanbul, Turkey.

(ii) a PN-aware Doppler CRB following the augmented-FIM approach in [9] (Theorem 3), revealing a velocity floor invisible to κ ; and (iii) a proof that the joint PA+PN CRB separates into an orthogonal (IBO, β) design space (Corollary 1)—absent from both [9] and [10]. All results are validated by Monte Carlo simulation and shown robust to practical DPD template errors.

Notation: Bold lowercase and uppercase denote vectors and matrices; $(\cdot)^H$ denotes Hermitian transpose; I_M is the $M \times M$ identity.¹

II. SYSTEM MODEL

A. OFDM-ISAC Signal Model

Consider a monostatic OFDM-ISAC system with N subcarriers at spacing Δf and M symbols per coherent processing interval (CPI), with symbol duration $T = 1/\Delta f + T_{\text{CP}}$ (Fig. 1). The transmitter communicates with a single-antenna user and senses a point target with delay τ , Doppler ν , and reflectivity α_s . The frequency-domain symbol $X[k, m]$ is drawn from a QAM constellation with energy $P_X = \mathbb{E}[|X[k, m]|^2]$. We define centered indices $k' = k - (N-1)/2$ and $m' = m - (M-1)/2$, and the per-subcarrier sensing SNR as $\gamma_s \triangleq |\alpha_s|^2 P_X / \sigma^2$, where σ^2 is the noise variance. The per-symbol aggregated sensing SNR used in the PN analysis is $\gamma_0 = 2N\gamma_s$ (the factor 2 arises from parameterizing $\alpha_s = \alpha_R + j\alpha_I$ as two real unknowns in the FIM). The target radial velocity is $v = \nu c / (2f_c)$ due to the monostatic two-way propagation.

B. PA Nonlinearity

The frequency-domain symbols are converted to time domain, passed through a memoryless PA, and transformed back: $x_m[n] = \frac{1}{\sqrt{N}} \sum_k X[k, m] e^{j2\pi kn/N}$, $z_m[n] = g(x_m[n])$, where $g(\cdot)$ is the PA input–output characteristic. We adopt the Rapp model [11]: $g(x) = x(1 + (|x|/A_{\text{sat}})^{2p})^{-1/(2p)}$ with saturation amplitude A_{sat} and smoothness factor p . The input back-off is $\text{IBO} = 10 \log_{10}(A_{\text{sat}}^2/P_X)$ dB. The PA output in frequency domain is $Z[k, m] = \frac{1}{\sqrt{N}} \sum_n z_m[n] e^{-j2\pi kn/N}$.

Crucially, since the transmitter generates $X[k, m]$ and applies $g(\cdot)$ digitally (or monitors the PA output via a digital pre-distortion (DPD) feedback path [12]), $Z[k, m]$ is a *deterministic, known* quantity at the sensing receiver—it is not noise. Theorem 1 holds for any memoryless PA model; the Rapp model is adopted only for numerical evaluation.

¹Additional notation: $(\cdot)^*$, $(\cdot)^T$ denote conjugate and transpose; $\text{Re}\{\cdot\}$ denotes the real part.

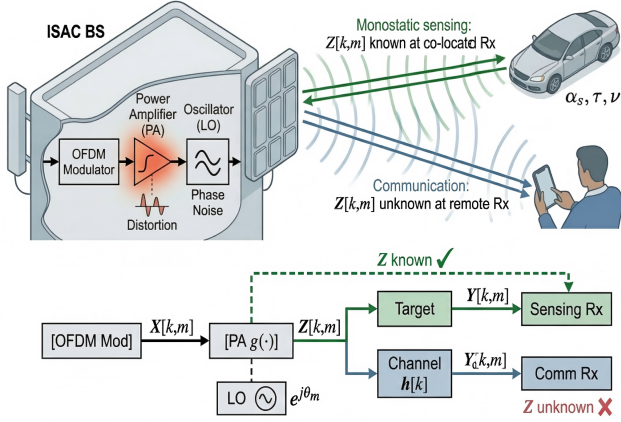


Fig. 1. Monostatic OFDM-ISAC system. *Upper*: The ISAC base station transmits PA-distorted, phase-noise-affected waveforms for simultaneous sensing and communication. *Lower*: Signal flow showing that $Z[k, m]$ is deterministically known at the co-located sensing receiver (✓) but unknown at the remote communication receiver (✗)—the asymmetry that the κ model fails to capture.

C. Phase Noise

The oscillator introduces a common phase error (CPE) per OFDM symbol [9], [13]:

$$\theta_m \approx \varphi(mT + T/2), \quad \theta \sim \mathcal{N}(\mathbf{0}, \mathbf{C}_\theta), \quad (1)$$

where $\varphi(t)$ is a Wiener process with 3-dB linewidth β , and $[\mathbf{C}_\theta]_{i,j} = \sigma_\Delta^2 \cdot \min(i+1, j+1)$ with $\sigma_\Delta^2 = 4\pi\beta T$. The CPE approximation is accurate when $\sigma_\Delta^2 \ll 1$; for our parameters ($\beta \leq 1$ kHz, $T \approx 8.9$ μ s), $\sigma_\Delta^2 \leq 0.12$, introducing $<5\%$ error at the highest linewidth. The ICI-aware model of [9] can be adopted for higher linewidths, where inter-subcarrier coupling modifies J_{τ, θ_m} and may weaken the delay–PN decoupling.

Following [9], θ represents accumulated phase from CPI start (worst case); shared-oscillator/short-range systems see partial TX–RX cancellation.

D. Observation Models

Sensing: Under both PA and PN, the monostatic observation is

$$Y[k, m] = \alpha_s e^{-j2\pi k' \Delta f \tau} e^{j2\pi \nu m' T} e^{j\theta_m} Z[k, m] + W[k, m], \quad (2)$$

where $W[k, m] \sim \mathcal{CN}(0, \sigma^2)$ is AWGN.

Communication: The user receives $Y_c[k, m] = h[k] e^{j\theta_m} Z[k, m] + W_c[k, m]$, where $h[k]$ is the channel frequency response and $W_c \sim \mathcal{CN}(0, \sigma_c^2)$. Unlike sensing, the communication receiver does *not* know $X[k, m]$ and hence cannot compute $Z[k, m]$.

III. PA-AWARE ANALYSIS

A. Physics-Based Sensing CRB

We first analyze PA in isolation ($\theta_m = 0$). Since $Z[k, m]$ is known, the observation (2) has known mean $\mu_{km} = \alpha_s e^{-j2\pi k' \Delta f \tau} e^{j2\pi \nu m' T} Z[k, m]$ and noise σ^2 . Applying the Slepian–Bangs formula [14] to the target parameter vector $\eta_d = [\tau, \nu, \alpha_R, \alpha_I]^T$ yields:

Theorem 1 (PA-Aware Sensing CRB). *The CRB for delay and Doppler estimation under PA nonlinearity is*

$$\text{CRB}^{\text{PA}}(\tau) = \frac{\sigma^2}{2|\alpha_s|^2 (2\pi \Delta f)^2 \tilde{E}_{20}^{(Z)}}, \quad (3)$$

$$\text{CRB}^{\text{PA}}(\nu) = \frac{\sigma^2}{2|\alpha_s|^2 (2\pi T)^2 \tilde{E}_{02}^{(Z)}}, \quad (4)$$

where $\tilde{E}_{20}^{(Z)} = \sum_{k,m} (k')^2 |Z[k, m]|^2$ and $\tilde{E}_{02}^{(Z)} = \sum_{k,m} (m')^2 |Z[k, m]|^2$ are spectral moments of the PA output. The degradation relative to the ideal case is $\Delta_{\text{sens}}^{\text{PA}} = 10 \log_{10}(\tilde{E}_{20}^{(X)} / \tilde{E}_{20}^{(Z)})$ dB, which is *SNR-independent*. For the Rapp model with $p = 3$ and 16-QAM, $\Delta_{\text{sens}}^{\text{PA}}$ remains below 1.1 dB for $\text{IBO} \geq 3$ dB.

Proof: Follows from the Slepian–Bangs formula with $Z[k, m]$ replacing $X[k, m]$ as the known waveform. Under centered indexing and approximately symmetric energy allocation, the off-diagonal coupling terms of the FIM are negligible (verified numerically: residual $< 10^{-4}$), yielding the diagonal CRB (3)–(4). ■

Physical insight: The small degradation (< 1.1 dB) occurs because PA spectral regrowth partially compensates the signal compression—the distortion energy adds useful high-frequency content to $\tilde{E}_{20}^{(Z)}$, partially offsetting the power loss.

B. κ /Bussgang Overestimation

The Bussgang decomposition [15] writes $Z[k, m] = \alpha_B X[k, m] + D[k, m]$, where $\alpha_B \triangleq \mathbb{E}[z x^*] / \mathbb{E}[|x|^2]$ is the linear gain and $\sigma_d^2 \triangleq \mathbb{E}[|z - \alpha_B x|^2]$ is the uncorrelated distortion variance, both estimated numerically from the time-domain PA input–output under Gaussian-distributed OFDM signals. We evaluate the standard aggregate κ model as used in [7], [8], which treats D as *unknown noise* in the sensing echo, yielding effective noise $\sigma_{\text{eff}}^2 = |\alpha_s|^2 \sigma_d^2 + \sigma^2$.

Theorem 2 (Overestimation Gap). *The ratio of the Bussgang CRB to the physics-based CRB satisfies*

$$\frac{\text{CRB}^B(\tau)}{\text{CRB}^{\text{PA}}(\tau)} = \underbrace{\frac{\tilde{E}_{20}^{(Z)}}{|\alpha_B|^2 \tilde{E}_{20}^{(X)}}}_{\approx 1} \cdot \underbrace{\left(1 + \frac{|\alpha_s|^2 \sigma_d^2}{\sigma^2}\right)}_{\text{spurious, } \propto \gamma_s}, \quad (5)$$

where the second factor grows linearly with γ_s , creating a false sensing floor.

Proof: Follows from the ratio of (3) to the Bussgang CRB, which substitutes $|\alpha_B|^2 \tilde{E}_{20}^{(X)}$ for $\tilde{E}_{20}^{(Z)}$ and uses noise σ_{eff}^2 . ■

C. Communication Under PA

For communication, the Bussgang model is correct: the receiver cannot reconstruct $Z[k, m]$. The achievable SINR is $\gamma_c^{\text{PA}} = |h|^2 |\alpha_B|^2 P_X / (|h|^2 \sigma_d^2 + \sigma_c^2)$, and the communication rate is $R = \log_2(1 + \gamma_c^{\text{PA}})$ bits/s/Hz.² The communication

² R represents an upper bound assuming Gaussian signaling on a flat-fading channel; achievable rates with finite-alphabet constellations over frequency-selective channels are lower, but the asymmetry conclusions (dB ratios) remain valid.

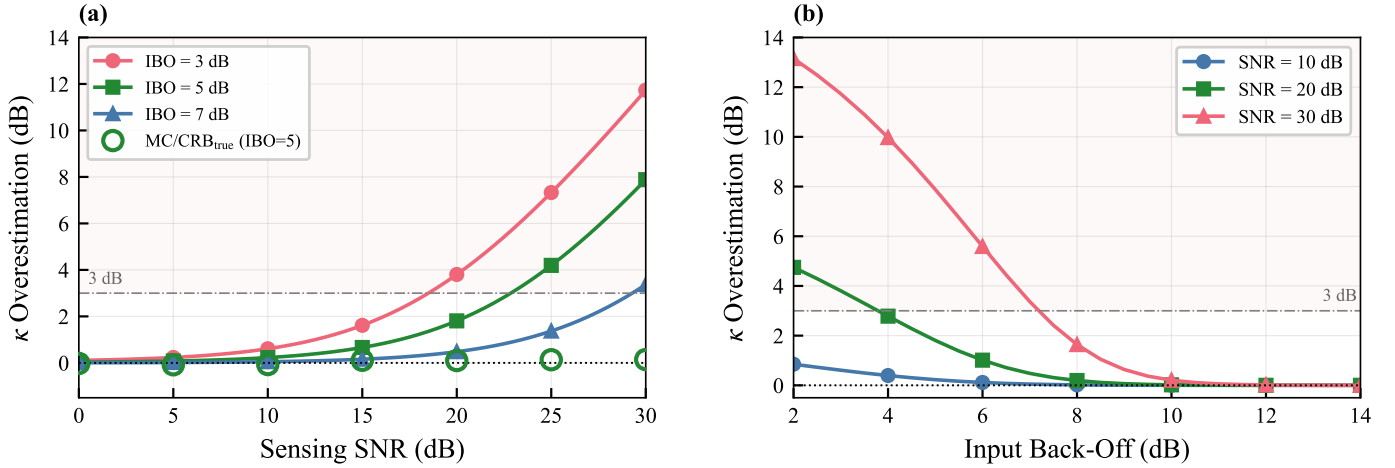


Fig. 2. PA sensing CRB analysis. (a) κ model overestimation ratio vs. SNR: the physics-based CRB is validated by MC (hollow circles near 0 dB); the κ model diverges at high SNR. (b) Overestimation vs. IBO at fixed SNR values.

degradation $\Delta_{\text{comm}}^{\text{PA}}$ grows with SNR due to a real distortion floor—in stark contrast to the SNR-independent sensing degradation.

IV. PN-AWARE ANALYSIS

A. Augmented FIM and Schur Complement

With PN, the parameter vector is augmented: $\boldsymbol{\eta} = [\boldsymbol{\eta}_d^T, \boldsymbol{\theta}^T]^T$. The random CPE $\boldsymbol{\theta}$ has prior $\mathcal{N}(\mathbf{0}, \mathbf{C}_\theta)$. The effective FIM for target parameters follows from the hybrid CRB [14]:

$$\mathbf{J}_{\text{eff}} = \mathbf{J}_{dd} - \mathbf{J}_{d\theta}(\mathbf{J}_{\theta\theta} + \mathbf{C}_\theta^{-1})^{-1}\mathbf{J}_{\theta d}, \quad (6)$$

where \mathbf{J}_{dd} , $\mathbf{J}_{d\theta}$, $\mathbf{J}_{\theta\theta}$ are blocks of the observation FIM.

Theorem 3 (PN-Aware Sensing CRB). *Under CPE phase noise with symmetric spectrum:*

- 1) **Delay** is unaffected: $\text{CRB}^{\text{PN}}(\tau) = \text{CRB}^{\text{ideal}}(\tau)$, since $J_{\tau, \theta_m} \propto \sum_k k' |X[k, m]|^2 = 0$ under symmetric spectrum.
- 2) **Doppler**: The effective FIM element is

$$J_{\nu\nu}^{\text{eff}} = \gamma_0 (2\pi T)^2 \mathbf{m}'^T (\gamma_0 \mathbf{C}_\theta + \mathbf{I}_M)^{-1} \mathbf{m}', \quad (7)$$

where $\gamma_0 = 2|\alpha_s|^2 E_s / \sigma^2 = 2N\gamma_s$ is the per-symbol aggregated SNR, with $E_s = \sum_k |X[k, m]|^2 = NP_X$.

- 3) **High-SNR floor**: As $\gamma_0 \rightarrow \infty$, $\text{CRB}_\infty^{\text{PN}}(\nu) = [(2\pi T)^2 \mathbf{m}'^T \mathbf{C}_\theta^{-1} \mathbf{m}']^{-1}$, an irreducible limit with the velocity floor scaling as $\sqrt{\beta}$.

Proof: The delay–PN coupling vanishes under symmetric spectrum ($J_{\tau, \theta_m} = 0$). For Doppler, the Schur complement (6) with $\mathbf{I} - \gamma_0(\gamma_0 \mathbf{I} + \mathbf{C}_\theta^{-1})^{-1} = (\gamma_0 \mathbf{C}_\theta + \mathbf{I})^{-1}$ yields (7). The floor follows from $(\gamma_0 \mathbf{C}_\theta + \mathbf{I})^{-1} \rightarrow (\gamma_0 \mathbf{C}_\theta)^{-1}$ as $\gamma_0 \rightarrow \infty$. ■

Physical insight: PN adds a random per-symbol phase θ_m indistinguishable from the Doppler phase $2\pi\nu mT$. At high SNR, the PN realization is estimated from data, masking the Doppler signature; only the PN prior resolves this ambiguity.

B. Joint PA+PN Separability

Under the joint observation model (2) with both PA and PN, the known waveform $Z[k, m]$ replaces $X[k, m]$ in the augmented FIM. Since $Z[k, m]$ is deterministic, the FIM block structure is preserved:

Corollary 1 (Orthogonal Design Space). *Under joint PA nonlinearity and CPE phase noise, the sensing CRB satisfies:*

- 1) **Delay**: $\text{CRB}^{\text{PA+PN}}(\tau) = \text{CRB}^{\text{PA}}(\tau)$, determined solely by IBO (PA spectral moments).
- 2) **Doppler floor**: $\text{CRB}_\infty^{\text{PA+PN}}(\nu) = [(2\pi T)^2 \mathbf{m}'^T \mathbf{C}_\theta^{-1} \mathbf{m}']^{-1}$, determined solely by β (PN statistics), independent of PA.
- 3) **Communication rate**: $R^{\text{PA+PN}} \approx R^{\text{PA}}$, determined solely by IBO, since PN contributes < 0.14 dB loss.

Proof: Replacing $X[k, m]$ by $Z[k, m]$ in Theorem 3, the per-symbol SNR becomes $\gamma_0^{(Z)} = 2|\alpha_s|^2 E_s^{(Z)} / \sigma^2$, where $E_s^{(Z)} = \sum_k |Z[k, m]|^2$. PA modifies only $E_s^{(Z)}$; the covariance \mathbf{C}_θ and symbol-index vector \mathbf{m}' are unchanged. In the Doppler floor regime ($\gamma_0^{(Z)} \mathbf{C}_\theta \gg \mathbf{I}_M$), the Schur complement (7) simplifies to $(2\pi T)^2 \mathbf{m}'^T \mathbf{C}_\theta^{-1} \mathbf{m}'$, where $\gamma_0^{(Z)}$ cancels. Thus the velocity floor depends exclusively on \mathbf{C}_θ (i.e., β), not on the PA output energy. For delay, $J_{\tau, \theta_m} \propto \sum_k k' |Z[k, m]|^2 \approx 0$ since PA, being memoryless and applied to real-valued envelopes, preserves the spectral symmetry of $|Z[k, m]|^2$ (verified numerically: residual $< 10^{-4}$ for $NM \geq 3584$). ■

Design implication: IBO controls rate (via σ_d^2) and β controls velocity (via \mathbf{C}_θ); the separability is exact for delay (all SNR) and the Doppler floor (high SNR), with residual coupling vanishing as SNR grows. Fig. 4 confirms this: velocity contours are horizontal, rate contours vertical.

C. Communication Under PN

Communication receivers estimate and remove θ_m using N_p pilot subcarriers, achieving residual variance $\sigma_\theta^2 = 1/(2N_p \gamma_c)$ at communication SNR γ_c [13]. At moderate-to-high SNR ($\gamma_c \gg 1$), the SINR loss converges to $\Delta_{\text{comm}}^{\text{PN}} \approx 10 \log_{10}(1 +$

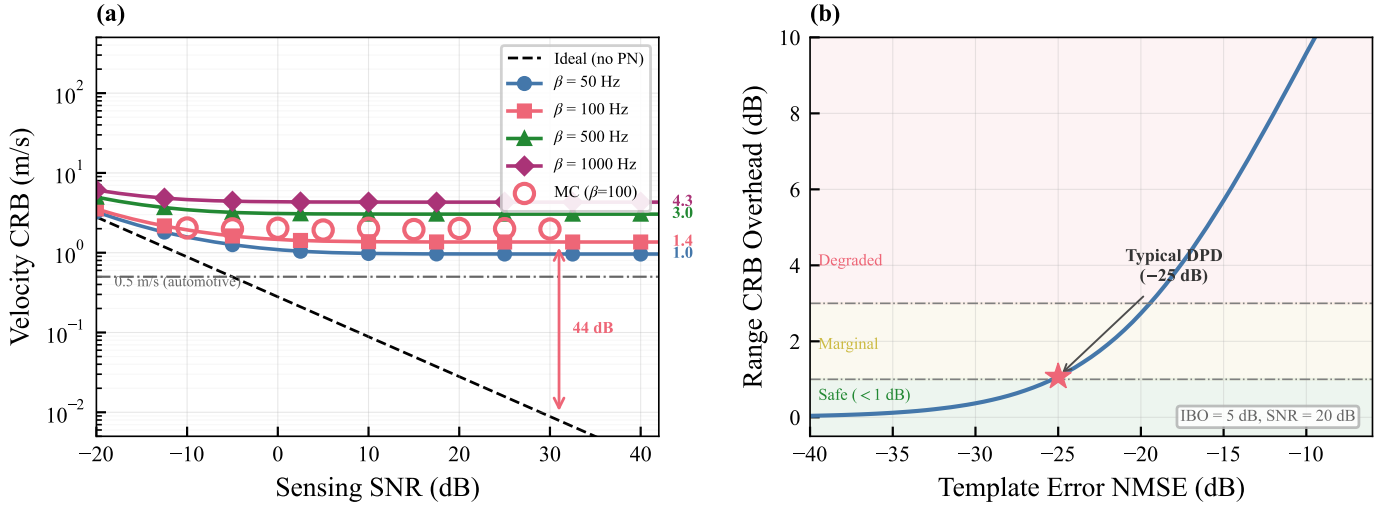


Fig. 3. (a) Velocity CRB vs. SNR: L-shaped curves reveal the transition from noise-limited to PN floor-limited regimes. The ideal baseline (dashed) diverges from all PN curves by >40 dB at high SNR. MC validates $\beta=100$ Hz. (b) DPD template error sensitivity: range CRB overhead vs. template NMSE at IBO = 5 dB, SNR = 20 dB. Star marks typical DPD accuracy (-25 dB).

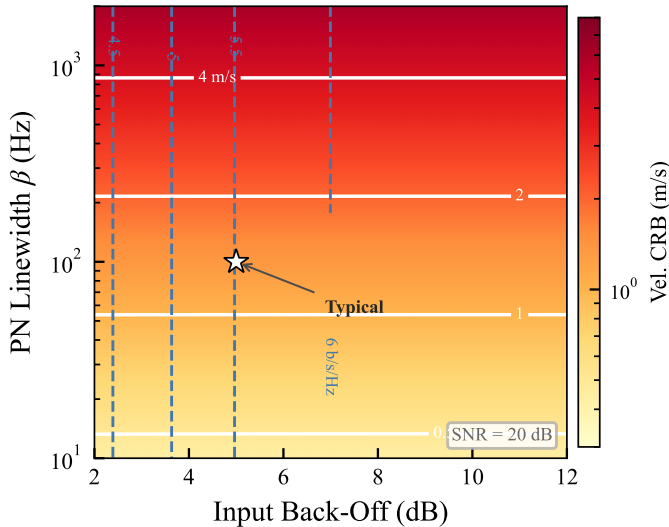


Fig. 4. Joint IBO- β design map at SNR = 20 dB. Color shows velocity CRB (m/s); white contours are velocity thresholds, blue dashed contours are communication rates (bits/s/Hz). Contour orthogonality directly visualizes the separability in Corollary 1. Star marks a typical operating point.

$1/(2N_p)$ dB, which is below 0.14 dB for $N_p \geq 16$. Thus, PN is effectively a sensing-only impairment at practical communication SNR.

V. NUMERICAL RESULTS

A. PA Overestimation

The system uses $N=256$, $M=14$, $\Delta f=120$ kHz ($T \approx 8.9$ μ s), 16-QAM, $f_c=28$ GHz, Rapp PA ($p=3$), Wiener CPE, IBO = 5 dB, $\beta=100$ Hz, and $N_p=16$. MC simulations use grid-search estimation with $N_{MC}=1500$ (PA) and 800 (PN) realizations.

B. PN Velocity Floor and DPD Robustness

Fig. 2(a) plots the κ model overestimation ratio versus sensing SNR. MC simulation (hollow circles, IBO = 5 dB) validates the physics-based CRB: the MC MSE fluctuates near 0 dB, with deviations attributable to finite-sample variance. The κ overestimation grows from <1 dB at low SNR to 12 dB at SNR = 30 dB with IBO = 3 dB; even at IBO = 7 dB, it reaches ~ 4 dB at 30 dB. Fig. 2(b) confirms that the overestimation exceeds 3 dB for IBO ≤ 8 dB at SNR = 30 dB, demonstrating that the κ model is unreliable across the practical operating region.

Fig. 3(a) plots the absolute velocity CRB versus sensing SNR. Each curve exhibits an L-shaped transition: at low SNR, the CRB follows the ideal (noise-limited) baseline, while at high SNR it saturates at a PN-induced floor that scales as $\sqrt{\beta}$ (Theorem 3), yielding floors of 0.96, 1.36, 3.04, and 4.30 m/s for $\beta = 50, 100, 500, 1000$ Hz—all exceeding the 0.5 m/s automotive requirement [2]. MC simulation ($\beta = 100$ Hz) validates the analytical CRB. The 44 dB gap between the ideal and $\beta=100$ Hz curves at SNR = 30 dB quantifies the wasted transmit power: beyond the PN-limited regime, increasing SNR yields no velocity improvement.

Fig. 3(b) examines the sensitivity of the range CRB to imperfect PA template knowledge. The overhead remains below 1 dB for template error NMSE ≤ -25 dB—the typical accuracy of practical DPD [12] (star)—and below 0.5 dB for NMSE ≤ -30 dB, validating that the “Z known” assumption is robust under practical calibration accuracy.

C. Joint IBO- β Design Map

Fig. 4 maps velocity CRB and communication rate jointly over the (IBO, β) design space at SNR = 20 dB. The velocity contours (white) are nearly horizontal (β -dominated) while the rate contours (blue) are nearly vertical (IBO-dominated), directly visualizing the orthogonal separability of Corollary 1. A system designer can independently specify the PA linearity

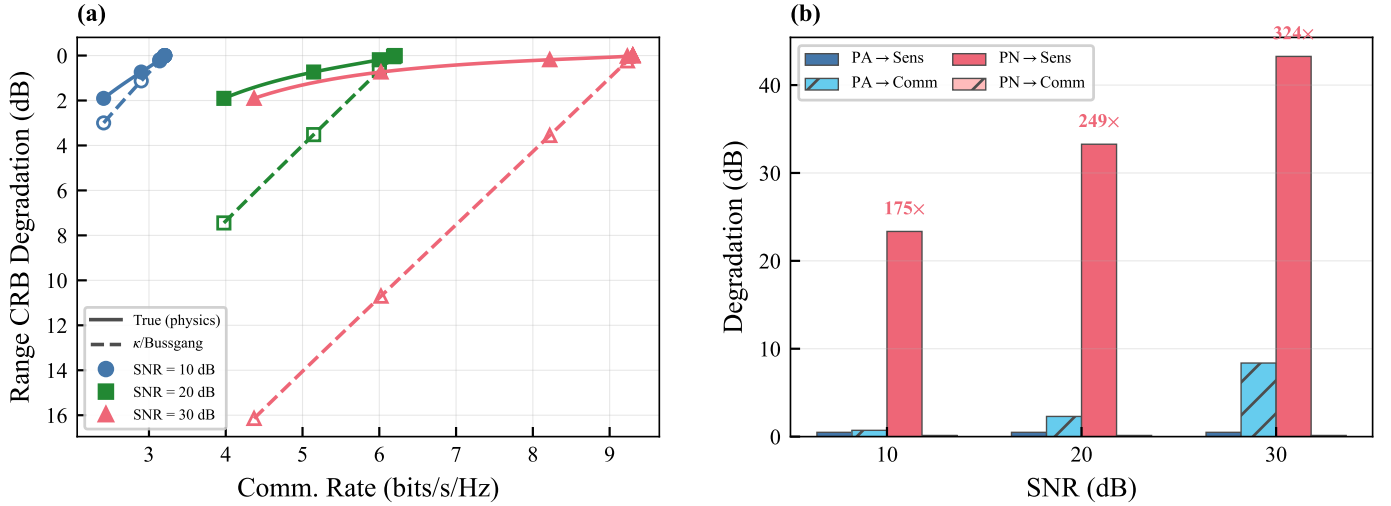


Fig. 5. (a) Sensing–communication Pareto frontier at SNR = 10, 20, 30 dB: the physics-based model (solid) shows significantly smaller sensing cost than the κ model (dashed), with the gap widening at higher SNR. (b) Bidirectional asymmetry (IBO = 5 dB, $\beta=100$ Hz): PA predominantly degrades communication while PN predominantly degrades sensing. Annotations show the sensing-to-communication degradation-factor ratio $10^{(\Delta_{\text{sens}} - \Delta_{\text{comm}})/10}$.

for communication and the oscillator quality for sensing. For example, at the typical operating point (star), relaxing PA linearity from IBO = 5 to 3 dB reduces the rate by 0.8 bits/s/Hz but changes the velocity CRB by <0.001 m/s; improving oscillator quality from $\beta = 100$ to 50 Hz halves the velocity CRB without affecting the rate.

D. Pareto Frontier and Asymmetry

Fig. 5(a) compares the sensing–communication Pareto frontiers under the physics-based and κ /Bussgang models at SNR = 10, 20, 30 dB. At each SNR, the true frontier (solid) lies well above the κ prediction (dashed), with the gap growing from <1 dB at 10 dB to ~ 8 dB at 30 dB—confirming that κ model pessimism worsens precisely where accurate sensing analysis matters most. Fig. 5(b) quantifies the bidirectional asymmetry at IBO = 5 dB: at SNR = 20 dB, PA degrades communication by 2.3 dB but sensing by only 0.49 dB, while PN degrades sensing by 33.3 dB but communication by only 0.13 dB, a gap of 33.2 dB.

VI. CONCLUSION

The κ distortion model is inadequate for monostatic sensing in ISAC: a physics-based analysis reveals a bidirectional asymmetry yielding an orthogonal (IBO, β) design space (Corollary 1), robust to practical DPD errors. PA linearity is primarily a communication requirement; oscillator quality is primarily a sensing requirement. Extension to MIMO, memory PA effects, I/Q imbalance, and multi-target scenarios is left for future work.

REFERENCES

- [1] F. Liu, Y. Cui, C. Masouros, J. Xu, T. X. Han, Y. C. Eldar, and S. Buzzi, “Integrated sensing and communications: Toward dual-functional wireless networks for 6G and beyond,” *IEEE J. Sel. Areas Commun.*, vol. 40, no. 6, pp. 1728–1767, Jun. 2022.
- [2] C. Sturm and W. Wiesbeck, “Waveform design and signal processing aspects for fusion of wireless communications and radar sensing,” *Proc. IEEE*, vol. 99, no. 7, pp. 1236–1259, Jul. 2011.
- [3] V. Koivunen, M. F. Keskin, H. Wymeersch, M. Valkama, and N. González-Prelcic, “Multicarrier ISAC: Advances in waveform design, signal processing, and learning under nonidealities,” *IEEE Signal Process. Mag.*, vol. 41, no. 5, pp. 17–30, Sep. 2024.
- [4] E. Björnson, M. Matthaiou, and M. Debbah, “A new look at dual-hop relaying: Performance limits with hardware impairments,” *IEEE Trans. Commun.*, vol. 61, no. 11, pp. 4512–4525, Nov. 2013.
- [5] T. C. W. Schenk, *RF Imperfections in High-Rate Wireless Systems: Impact and Digital Compensation*. Springer, 2008.
- [6] C. Studer, M. Wenk, and A. Burg, “MIMO transmission with residual transmit-RF impairments,” in *Proc. Int. ITG Workshop Smart Antennas (WSA)*, Bremen, Germany, Feb. 2010, pp. 189–196.
- [7] M. B. Salman, E. Björnson, and O. T. Demir, “Hardware distortion aware precoding for ISAC systems,” in *Proc. Asilomar Conf. Signals, Syst., Comput.*, Pacific Grove, CA, USA, Oct. 2025, pp. 1–5.
- [8] J. M. Mateos-Ramos, C. Häger, M. F. Keskin, L. Le Magoarou, and H. Wymeersch, “Model-based end-to-end learning for multi-target integrated sensing and communication under hardware impairments,” *IEEE Trans. Wireless Commun.*, vol. 24, no. 3, pp. 2574–2589, Mar. 2025.
- [9] M. F. Keskin, H. Wymeersch, and V. Koivunen, “Monostatic sensing with OFDM under phase noise: From mitigation to exploitation,” *IEEE Trans. Signal Process.*, vol. 71, pp. 3683–3698, 2023.
- [10] H. Dong and O. B. Akan, “Performance limits of hardware-constrained THz inter-satellite MIMO-ISAC systems,” *arXiv preprint arXiv:2512.13652*, 2025.
- [11] C. Rapp, “Effects of HPA-nonlinearity on a 4-DPSK/OFDM-signal for a digital sound broadcasting system,” in *Proc. 2nd Eur. Conf. Satellite Commun.*, Liège, Belgium, Oct. 1991, pp. 179–184.
- [12] F. M. Ghannouchi and O. Hammi, “Behavioral modeling and predistortion,” *IEEE Microw. Mag.*, vol. 10, no. 7, pp. 52–64, Dec. 2009.
- [13] S. Wu and Y. Bar-Ness, “OFDM systems in the presence of phase noise: Consequences and solutions,” *IEEE Trans. Commun.*, vol. 52, no. 11, pp. 1988–1996, Nov. 2004.
- [14] H. L. Van Trees, K. L. Bell, and Z. Tian, *Detection, Estimation, and Modulation Theory, Part I*, 2nd ed. Wiley, 2013.
- [15] J. J. Bussgang, “Crosscorrelation functions of amplitude-distorted Gaussian signals,” MIT Res. Lab. Electron., Tech. Rep. 216, Mar. 1952.